

Quantitative Analysis of Incipient Mineral Loss in Hard Tissues

Anna Matvienko^{a,b}, Andreas Mandelis*^{a,b}, Adam Hellen^{a,b}, Raymond Jeon^{a,b}, Stephen Abrams^b,
Bennett Amaechi^c

^aCenter for Advanced Diffusion-Wave Technologies, Department of Mechanical and Industrial Engineering, University of Toronto, 5 King's College Road, Toronto, ON M5S 3G8, Canada;

^bQuantum Dental Technologies Inc., 748 Briar Hill Ave, Toronto, ON M6B 1L3, Canada;

^cDepartment of Community Dentistry, University of Texas Health Science Center at San Antonio, 7703 Floyd Curl Drive, San Antonio, Texas 78229-3900, USA

ABSTRACT

A coupled diffuse-photon-density-wave and thermal-wave theoretical model was developed to describe the biophotonic phenomena in multi-layered hard tissue structures. Photothermal Radiometry was applied as a safe, non-destructive, and highly sensitive tool for the detection of early tooth enamel demineralization to test the theory. Extracted human tooth was treated sequentially with an artificial demineralization gel to simulate controlled mineral loss in the enamel. The experimental setup included a semiconductor laser (659 nm, 120 mW) as the source of the photothermal signal. Modulated laser light generated infrared blackbody radiation from teeth upon absorption and non-radiative energy conversion. The infrared flux emitted by the treated region of the tooth surface and sub-surface was monitored with an infrared detector, both before and after treatment. Frequency scans with a laser beam size of 3 mm were performed in order to guarantee one-dimensionality of the photothermal field. TMR images showed clear differences between sound and demineralized enamel, however this technique is destructive. Dental radiographs did not indicate any changes. The photothermal signal showed clear change even after 1 min of gel treatment. As a result of the fittings, thermal and optical properties of sound and demineralized enamel were obtained, which allowed for quantitative differentiation of healthy and non-healthy regions. In conclusion, the developed model was shown to be a promising tool for non-invasive quantitative analysis of early demineralization of hard tissues.

Keywords: Photothermal, dental, optical properties, thermal properties

1. INTRODUCTION

Recent developments in laser based medical and dental techniques have lead to an increasing need for accurate data on the optical and thermal properties of biological tissues. During the past decade, a number of *in vivo* methodologies for optical evaluation have been reported.¹⁻³ These techniques apply diffusion approximation of transport theory⁴ to convert measured optical reflectance or transmittance to the optical characteristics of tissues: absorption coefficient, scattering coefficient, and the mean cosine of scattering angle. Typically, a semi-infinite homogeneous tissue is assumed, and the solution of the diffusion equation at the surface, subject to appropriate boundary conditions, is calculated. However, many tissues are in fact multi-layered. It was shown that the single-layer approximation can lead to significant errors in the optical evaluation of layered tissues.⁵ On the other hand, introducing two different sets of optical coefficients for each layer and additional unknown thickness of the upper layer increases the complexity of the fitting procedure, where several sets of coefficients can give good approximation of the measured data simultaneously. In this case the robustness of the fitting algorithm is of great importance.

Several algorithms for extracting optical properties from the reflectance data of two-layered system were investigated: Marquardt-Levenberg nonlinear least squares algorithm,^{5,6} Newton-Raphson and neural network algorithms,⁵ and the simulated annealing minimization.⁷ The described algorithms require an initial set of optical properties as input parameters. However, the main problem of the fitting analysis of biological measurements is that the true values of properties may vary greatly within the same type of tissue. In this case, the range of the initial properties may vary, and the sensitivity of the algorithm to the change in the initial values eventually defines the accuracy of the fittings.

*mandelis@mie.utoronto.ca

Another group of methods for tissue evaluation use the secondary signal generated due to the light absorption, usually thermal⁸ or acoustic signal⁹ to measure the optical coefficients. The introduction of the secondary signal enhances the sensitivity of the measurements increasing the possibilities for the detection of early changes in tissues. However, the additional parameters, e.g. thermal properties of tissues, must be known in order to fit the theoretical curves representing thermal or acoustic signals. There are several published studies on the measurement of thermal properties of biological tissues.^{10,11} However, since the thermal properties can also vary among the same types of tissues, there is a need for the simultaneous measurement of optical and thermal properties for secondary-signal methods. Coupled with the fact that biological tissues are usually layered structures, the analysis becomes even more complicated.

Frequency-domain photothermal radiometry has recently shown the potential to provide simultaneous quantitative analysis of optical and thermal fields in multi-layered dental tissue structures.¹² This noninvasive and highly sensitive technique is superior to its pulsed version since it does not require the high-fluency deposition of laser energy for time-resolved analysis. The technique has already shown its capabilities for the non-invasive optical evaluation of dental tissues.¹³ The authors, however, considered single-layer approximation and extracted only the optical properties.

In this study, we apply frequency-domain photothermal radiometry (PTR) to evaluate optical and thermal properties of teeth as multi-layered structures. We measured the amplitude and phase of the PTR signal and apply Simplex Downhill algorithm for the multi-parameter fits of the properties. The theoretical profiles are generated with the coupled diffuse-photon-density wave and thermal wave model for the multi-layered turbid structures.¹² The fits were performed for the healthy and the artificially demineralized teeth. Separate sets of properties were fitted for different treatment time, allowing the analysis of the influence of the demineralization on the change of tissue properties and structure of the layers. The study showed the potential of PTR to quantitatively evaluate early tooth enamel demineralization in-vivo.

2. THEORETICAL MODEL

The theoretical approach is described in detail in our previous study.¹² We assume that a three-layered one-dimensional turbid structure is irradiated with laser light (Fig. 1).

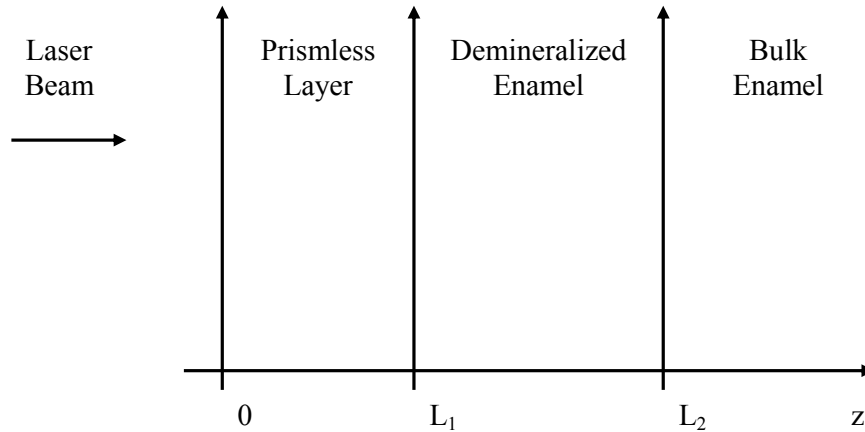


Fig. 1. Schematic tooth structure.

As a result of the incident radiation, a one-dimensional photon field density Ψ_{t_i} arises in the medium. Here, the subscript i denotes each layer of the dental structure (Fig. 1). The first layer of the structure is the prismless layer.^{14,15} The second layer is the demineralized layer, and the third is the healthy enamel layer. The healthy enamel layer was considered semi-infinite to simplify the analysis. To verify this approach, simulations were performed with optical and thermal properties of healthy enamel, obtained from literature data (Table 1). The simulations showed that the layer

thickness does not affect the calculated PTR curve at the frequency range above 8 Hz. The measured data in this frequency range were then chosen for the theoretical fits.

The general solutions for the optical fields for each layer ($i = 1,2,3$), including coherent and diffuse components, can be written as:¹²

$$\Psi_{t_1}(z) = a_1 \exp(Q_1 z) + b_1 \exp(-Q_1 z) + I_{eff} (1 + C_{\mu_1}) \left\{ \exp[-\mu_{t_1} z] + R_2 \exp[-\mu_{t_1} (2L_1 - z)] \right\} \quad (1a)$$

$$\Psi_{t_2}(z) = a_2 \exp[Q_2 (z - L_1)] + b_2 \exp[-Q_2 (z - L_1)] + I_{eff} (1 + R_2) (1 + C_{\mu_2}) \exp(-\mu_{t_1} L_1) \exp[-\mu_{t_2} (z - L_1)] \quad (1b)$$

$$\Psi_{t_3}(z) = b_3 \exp\{-Q_3 [z - (L_1 + L_2)]\} + I_{eff} (1 + R_2) (1 + C_{\mu_3}) \exp[-(\mu_{t_1} L_1 + \mu_{t_2} L_2)] \exp\{-\mu_{t_3} [z - (L_1 + L_2)]\} \quad (1c)$$

where the integration constants due to the coherent field solutions are given by:

$$C_{\mu_i} = \frac{3\mu_{s_i} (\mu_{t_i} + g\mu_{a_i})}{3\mu_{a_i} \mu_{t_i}' - \mu_{t_i}^2}, \quad (2)$$

$$I_{eff} = \frac{I_0 (1 - R_1)}{1 - R_1 R_2 \exp(-2\mu_{t_1} L_1)}$$

Here, I_0 is the laser intensity, R_1 is the reflectivity of the outermost turbid medium, R_2 is the reflectivity of the second layer, $\mu_{t_i} = \mu_{a_i} + \mu_{s_i}$ is the total attenuation coefficient of layer i , which includes the absorption coefficient μ_{a_i} , [m^{-1}], and the scattering coefficient μ_{s_i} , [m^{-1}], of the medium, and $\mu_{t_i}' = \mu_{a_i} + (1 - g)\mu_{s_i}$ is the reduced attenuation coefficient. g is the mean cosine of the scattering angle.

Applying the third-kind boundary conditions at the air-tooth interface, and the continuity of photon-density field and photon flux at the interfaces between solid layers, the system can be solved to obtain the coefficients a_1, a_2, b_1, b_2, b_3 :¹²

$$a_1 = \frac{-d_1 P - f_1 N \exp(-2\mu_{t_1} L_1) - \frac{(2VF + G) \exp(Q_1 L_1)}{(1 + X_{12} - 2VX_{12})}}{M - \frac{(1 - X_{12} + 2VX_{12}) \exp(2Q_1 L_1)}{(1 + X_{12} - 2VX_{12})}};$$

$$b_1 = -a_1 M - d_1 P - f_1 N \exp(-2\mu_{t_1} L_1);$$

$$a_2 = b_2 + d_2 Y_{22} + X_{12} a_1 \exp(Q_1 L_1) - X_{12} b_1 \exp(-Q_1 L_1) + Y_{12} (f_1 - d_1) \exp(-\mu_{t_1} L_1); \quad (3)$$

$$b_2 = VF - VX_{12} a_1 \exp(Q_1 L_1) + VX_{12} b_1 \exp(-Q_1 L_1);$$

$$b_3 = -a_2 X_{23} \exp(Q_1 L_1) + b_2 X_{23} \exp(-Q_1 L_1) + Y_{23} d_2 \exp(-\mu_{t_2} L_2) - Y_{33} d_3;$$

Here, the parameters $M, N, P, X, Y,$ and d are defined as:

$$M \equiv \frac{1-Q_1A}{1+Q_1A}, \quad N \equiv \frac{1-\mu_1A}{1+Q_1A}, \quad P \equiv \frac{1+\mu_1A}{1+Q_1A},$$

$$X_{ij} \equiv \frac{D_i Q_i}{D_j Q_j}, \quad Y_{ij} \equiv \frac{D_i \mu_i}{D_j Q_j},$$

$$d_1 = C_{\mu_1} I_{eff}, \quad f_1 = d_1 R_2, \quad d_2 = C_{\mu_2} I_{eff} (1 + R_2) \exp(-\mu_1 L_1), \quad (4)$$

$$d_3 = C_{\mu_3} I_{eff} (1 + R_2) \exp[-(\mu_1 L_1 + \mu_2 L_2)].$$

Here, the constant A is defined as:¹⁶

$$A = 2D \left(\frac{1+r}{1-r} \right) \quad (5)$$

where r is the internal reflection of uniformly diffusing radiation, which depends on the index of refraction of the sample.¹⁷ D represents the mean free path of photons limited by absorption and scattering.

The coefficients F, G and V are defined as:

$$F = d_2 \frac{\exp(-\mu_2 L_2)(Y_{23} - 1)}{\exp(Q_2 L_2)(X_{23} + 1)} + d_3 \frac{\exp(1 - Y_{33})}{\exp(Q_2 L_2)(X_{23} + 1)} - d_2 Y_{22} - (f_1 - d_1) Y_{12} \exp(-\mu_1 L_1);$$

$$G = -(f_1 + d_1) \exp(-\mu_1 L_1) + d_1 + d_2 Y_{22} + (f_1 - d_1) Y_{12} \exp(-\mu_1 L_1); \quad (6)$$

$$V = \frac{1}{1 - \frac{(X_{23} - 1)}{(X_{23} + 1)} \exp(-2Q_2 L_2)}.$$

The optical field is a source of the thermal field in the sample. The thermal-wave fields for each layer can be written in the form:¹²

$$T_1(z; \omega) = A_1 \exp(\sigma_1 z) + B_1 \exp(-\sigma_1 z) + C_1 \exp(Q_1 z) + D_1 \exp(-Q_1 z) + E_1 \exp(-\mu_1 z) + F_1 \exp[-\mu_1 (2L_1 - z)]; \quad (7a)$$

$$T_2(z; \omega) = A_2 \exp[\sigma_2 (z - L_1)] + B_2 \exp[-\sigma_2 (z - L_1)] + C_2 \exp[Q_2 (z - L_1)] + D_2 \exp[-Q_2 (z - L_1)] + E_2 \exp[-\mu_2 (z - L_1)]; \quad (7b)$$

$$T_3(z; \omega) = B_3 \exp\{-\sigma_3 [z - (L_1 + L_2)]\} + D_3 \exp\{-Q_3 [z - (L_1 + L_2)]\} + E_3 \exp\{-\mu_3 [z - (L_1 + L_2)]\}; \quad (7c)$$

where

$$\sigma_i = \sqrt{\frac{i\omega}{\alpha_i}} \quad (8)$$

is the thermal wavenumber, [m^{-1}], which depends on the modulation frequency and on thermal diffusivity α_i [m^2s^{-1}], of i -th layer. Here, η_{NR} is the non-radiative efficiency and κ is the thermal conductivity of the i -th layer, [$\text{Wm}^{-1}\text{K}^{-1}$].

The coefficients C_i , D_i , E_i and F_i are defined as:

$$\begin{aligned} C_i &= -\frac{\eta_{NR_i} \mu_{a_i}}{\kappa_i (Q_i^2 - \sigma_i^2)} a_i; \quad i = 1, 2 \\ D_i &= -\frac{\eta_{NR_i} \mu_{a_i}}{\kappa_i (Q_i^2 - \sigma_i^2)} b_i; \quad i = 1, 2, 3 \\ E_i &= -\frac{\eta_{NR_i} \mu_{a_i}}{\kappa_i (\mu_i^2 - \sigma_i^2)} d_i; \quad i = 1, 2, 3 \\ F_i &= -\frac{\eta_{NR_i} \mu_{a_i}}{\kappa_i (\mu_i^2 - \sigma_i^2)} f_i. \end{aligned} \quad (9)$$

Here, a_i , b_i , d_i , f_i are given in Eqs. (3) and (4).

The coefficients of the photothermal fields T_1 , T_2 , T_3 in Eqs. (7) can be found from the solution of the following system of equations:¹²

$$\begin{aligned} A_1(1 - b_{01}) - B_1(1 + b_{01}) &= C_1(b_{01} - q_{11}) + D_1(b_{01} + q_{11}) + E_1(b_{01} + m_{11}) \\ &\quad + F_1 \exp(-\mu_1 L_1)(b_{01} - m_{11}); \\ A_1 \exp(\sigma_1 L_1) + B_1 \exp(-\sigma_1 L_1) - A_2 - B_2 &= C_2 + D_2 + E_2 \\ &\quad - C_1 \exp(Q_1 L_1) - D_1 \exp(-Q_1 L_1) - (E_1 + F_1) \exp(-\mu_1 L_1); \\ b_{12} A_1 \exp(\sigma_1 L_1) - b_{12} B_1 \exp(-\sigma_1 L_1) - A_2 + B_2 &= \\ q_{22} C_2 - q_{22} D_2 - m_{22} E_2 - q_{12} C_1 \exp(Q_1 L_1) + q_{12} D_1 \exp(-Q_1 L_1) & \\ - m_{12} (F_1 - E_1) \exp(-\mu_1 L_1); & \\ A_2 \exp(\sigma_2 L_2) + B_2 \exp(-\sigma_2 L_2) + B_3 &= \\ - C_2 \exp(Q_2 L_2) - D_2 \exp(-Q_2 L_2) - E_2 \exp(-\mu_2 L_2) - D_3 - E_3; & \\ q_{23} A_2 \exp(\sigma_2 L_2) - q_{23} B_2 \exp(-\sigma_2 L_2) + B_3 &= \\ - q_{23} C_2 \exp(Q_2 L_2) + q_{23} D_2 \exp(-Q_2 L_2) + m_{22} E_2 \exp(-\mu_2 L_2) - q_{33} D_3 - m_{33} E_3; & \end{aligned} \quad (10)$$

where the following definitions are used:

$$b_{ij} \equiv \frac{\kappa_i \sigma_i}{\kappa_j \sigma_j}, \quad q_{ij} \equiv \frac{\kappa_i Q_i}{\kappa_j \sigma_j}, \quad m_{ij} \equiv \frac{\kappa_i \mu_i}{\kappa_j \sigma_j}. \quad (11)$$

The photothermal radiometric (PTR) signal represents the overall Plank radiation emission integrated over the depth of the sample:

$$V_{PTR}(\omega) = C(\omega) \mu_{IR} \left[\int_0^{L_1} T(z, \omega) e^{-\mu_{IR} z} dz + \int_{L_1}^{L_2} T(z, \omega) e^{-\mu_{IR} z} dz + \int_{L_2}^{\infty} T(z, \omega) e^{-\mu_{IR} z} dz \right] \quad (12)$$

Here, μ_{IR} is the spectrally averaged effective infrared absorption of the medium. The instrumental transfer function $C(\omega)$ was calculated based on the fitting the PTR signal measured with the thermally thick glassy carbon sample [diameter 40 mm, thickness 10 mm, Grade GC-20SS, Tokai Carbon Co., Ltd, Japan] with known thermal properties to the theoretical signal calculated for the semi-infinite opaque solid.¹⁸

3. MATERIALS AND METHODS

Extracted human tooth (third molar) selected for the study had healthy surface with no visible defects, stains, restorations, or cracks. Sample was carefully cleaned with a toothbrush and polishing paste (Temrex), mounted on a LEGO block (15.8 mm(W) × 15.8 mm(D) × 9.5 mm(H)), and stored in an air-tight humid container before measurements. Mounting tooth on a LEGO block allowed remounting into the exact position during repeated measurements.

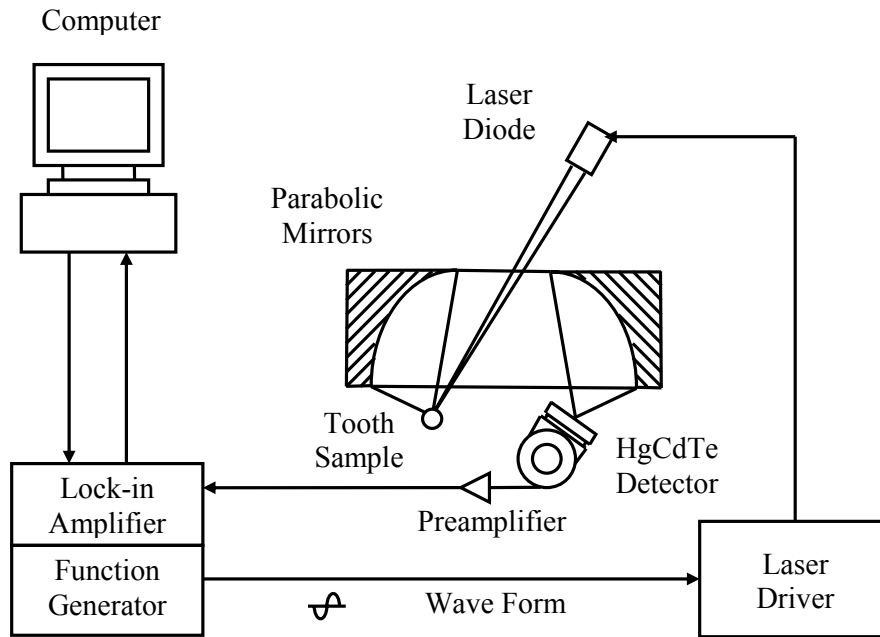


Fig. 2. Experimental setup.

Demineralization of the sample was carried out in 25 ml of treatment solution in a 50-ml polypropylene test tube, with the sample immersed upside down such that only the tooth would be immersed. Demineralization to create caries-like lesions was achieved using an acidified gel system,¹⁹ consisting of 0.1 M lactic acid solution gelled to a thick consistency with 6 % w/v hydroxyethylcellulose (Aldrich, Dorset, UK) and the pH adjusted to 4.5 with 0.1 M NaOH. After treatment, sample was rinsed under running tap water for approximately 1 min and dried in air for 5 minutes (was it 5min, or did we leave it out for 1 hour to dry). The sample was treated with the demineralization time periods of 1 min, 1 day, 3 days, 7 days and 14 days. The tooth was taken out of the container about 20 minutes before each experiment for drying, in order to avoid causing signal drift due to small humidity changes on the enamel surface. Then, the tooth on the

LEGO base was placed on the micro-positioning stage, the laser was turned on and another 10 minutes lapsed before measurements commenced, so that the sample surface was stabilized thermally.

The PTR experimental setup is shown in Fig. 2. A semiconductor laser diode emitting at 659 nm (Mitsubishi ML101J27, maximum power: 120 mW) was used as the source of the PTR signal. The diameter of the laser beam was approx. 3 mm to ensure the one-dimensionality of the photothermal field. A diode laser driver (Thorlab, LDC 210) was triggered by the built-in function generator of the lock-in amplifier (EG&G 7265) to modulate the laser current harmonically. The modulated infrared PTR signal from the tooth was collected and focused by two off-axis paraboloidal mirrors (Melles Griot 02POA017, Rhodium coated) onto a Mercury Cadmium Telluride (HgCdTe or MCT) detector (Judson Technologies J15D12, spectral range: 2 to 12 μm , peak detectivity $D^* \approx 5 \times 10^{10} \text{ cm Hz}^{1/2} \text{ W}^{-1}$ at ca. 12 μm). Before being sent to the lock-in amplifier, the PTR signal was amplified by a preamplifier (Judson Technologies PA-300). The lock-in amplifier was controlled by computer via RS-232 ports.

The experiments consisted of frequency scans measuring the amplitude and the phase of the PTR signal at the treated area by varying the frequency from 8 Hz to 100 Hz. There was a 15-s time delay between each frequency step to allow for thermalization of the tooth surface.

Following completion of the PTR measurements, the sample was subjected to Transverse microradiography (TMR) analysis to determine the mineral loss and the depth of the carious lesion. The sample was carefully sectioned, using a water-cooled diamond-coated wire saw model 3242 (Well, Le Locle, Switzerland), to produce an enamel slice approximately 100- μm thick from the lesion area. The slice, together with an aluminum step wedge (10 steps of 24.5 μm thickness), was microradiographed on type 1A high resolution glass X-ray plates (IMTECH CA, USA) with a Phillips x-ray generator system equipped with a nickel filtered Cu-K α target, producing monochromatic radiation of wavelength appropriate for hydroxyapatite (184 \AA). The plates were exposed for 10 minutes at 20kV/10 mA, and processed. Processing consists of a 5-minute development in a developer (Kodak HR) and 15 min fixation in a Rapid-fixer (Kodak) before a final 30-minute wash period. After drying, the microradiographs were visualized using a DMR optical microscope (Leica) linked via a CCTV camera (Sony, XC-75CE) to a computer (90 MHz Dell™ Pentium). The enhanced image of the microradiograph was analyzed under standard conditions of light intensity and magnification and processed, along with data from the image of the step wedge, using the TMR software (TMRW version 2.0.27.2, Inspektor Research Inc., Amsterdam, Netherlands)²⁰ to quantify the lesion parameters of integrated mineral loss (Δz , vol% μm) and lesion depth (LD, μm). The mineral loss was computed as the difference in volume percent of mineral between sound and demineralized tissue integrated over the lesion depth. The lesion depth was assessed as the distance from the measured sound enamel surface to the location in the lesion at which the mineral content is larger than 95% of the mineral content in sound enamel.

4. RESULTS AND DISCUSSION

One difficulty involving multi-parameter fitting procedures is that the solution of the problem is usually not unique, i.e., multiple combinations of parameters can fit the data almost equally well. Therefore, the robustness of the fitting algorithm, i.e., its independence of the initial estimation of parameters, becomes extremely important. In our fitting procedure, we used the range of initial values within the limits based on literature values^{15,21-23} as an initial guess for the fitting of each parameter (Table 1). The possible ranges for the optical and thermal parameters of the prismless layer and demineralized layer were increased compared to the bulk enamel, since the different orientation of the enamel crystals can significantly change the optical properties.

During the fits, we divided the set of these ranges by equal steps, and performed the fits for every combination of points for every parameter. These combinations of values became the initial estimations for the fits. The thorough investigation of dependence of the fitting results on the different combinations is the subject of our future investigation. In this study, we chose the set of data which resulted in the best fits (minimal residual) among the fits with different refining step from 1 to 25 divisions between the limits. The further refining of the initial grid was difficult to afford due to significant increase in the calculation time.

Our experimental PTR data were fitted using Simplex Downhill algorithm for the multi-parameter minimization.²⁴ The amplitude and phase of the PTR signal were both fitted to the theory, and the combined residual represented the criterion

for the best fits. The simultaneous use of two signals, the salient feature of the frequency-domain methods, doubles the amount of information gathered in a single set of scans compared to the time-domain techniques, increasing the validity of the fits. The residual was defined as follows:

$$Res = \frac{\sum_{n=1}^{n_{\max}} \left[\text{Log}_{10} (Amp_{Exp}) - \text{Log}_{10} (Amp_{Theor}) \right]^2 + \sum_{n=1}^{n_{\max}} \left[Phase_{Exp} - Phase_{Theor} \right]^2}{\sum_{n=1}^{n_{\max}} \left[\text{Log}_{10} (Amp_{Exp}) \right]^2 + \sum_{n=1}^{n_{\max}} \left[Phase_{Exp} \right]^2} \quad (13)$$

where Amp_{Exp} and $Phase_{Exp}$ are the measured PTR amplitude and phase, Amp_{Theor} and $Phase_{Theor}$ are the calculated data, and n_{\max} is the number of the frequency-scan points. Due to the large change in amplitude during experiments, the amplitude values were analyzed on a logarithmic scale.

Table. 1. Upper and lower limits for the initial guess of parameters (bulk enamel).

| | Upper Limit | Lower Limit | Reference |
|---|----------------------|-----------------------|-----------|
| Absorption coefficient, μ_{a3}, m^{-1} | 1 | 100 | 21 |
| Scattering coefficient, μ_{s3}, m^{-1} | 4000 | 8000 | 21 |
| Thermal diffusivity, $\alpha_3, \text{W/mK}$ | 4.2×10^{-7} | 4.69×10^{-7} | 22, 23 |
| Thermal conductivity, $\lambda_3, \text{W/mK}$ | 0.910 | 0.926 | 22, 23 |
| Non-radiative efficiency, η_{IR3} | 0 | 1 | |
| IR absorption coefficient, μ_{IR}, m^{-1} | 30000 | 200000 | 13 |
| Prismless layer thickness, $L_1, \mu\text{m}$ | 5 | 60 | 15 |
| Mean cosine angle, g | 0.94 | 0.98 | 21 |
| Reflectance of enamel layer, R_3 | 0 | 1 | |

The fitting of the curves for the different treatment times was conducted as follows. First, the data corresponding to the intact tooth scans were fitted. The model in this case considered the prismless layer and the bulk enamel only. The obtained optical and thermal parameters, as well as the thickness of the prismless layer were further used for the fits of the curves for 1 min and 1 day treatment, where the initial guess for the prismless layer thickness was varied between 0 mm and the thickness obtained for the intact tooth. Again, only the prismless layer and bulk enamel were taken into

consideration. It was done according to the multiple observations that demineralization begins only after several days of treatment. During the first few (1-3) days, the thickness of the prismless layer was continuously removed, which caused amplitude and phase curves to decrease. This can be explained by the fact that a smaller number of photons are captured by this layer as the thickness decreases. Consequently, the amount of energy converted to heat is smaller, resulting in a decrease in signal amplitude.

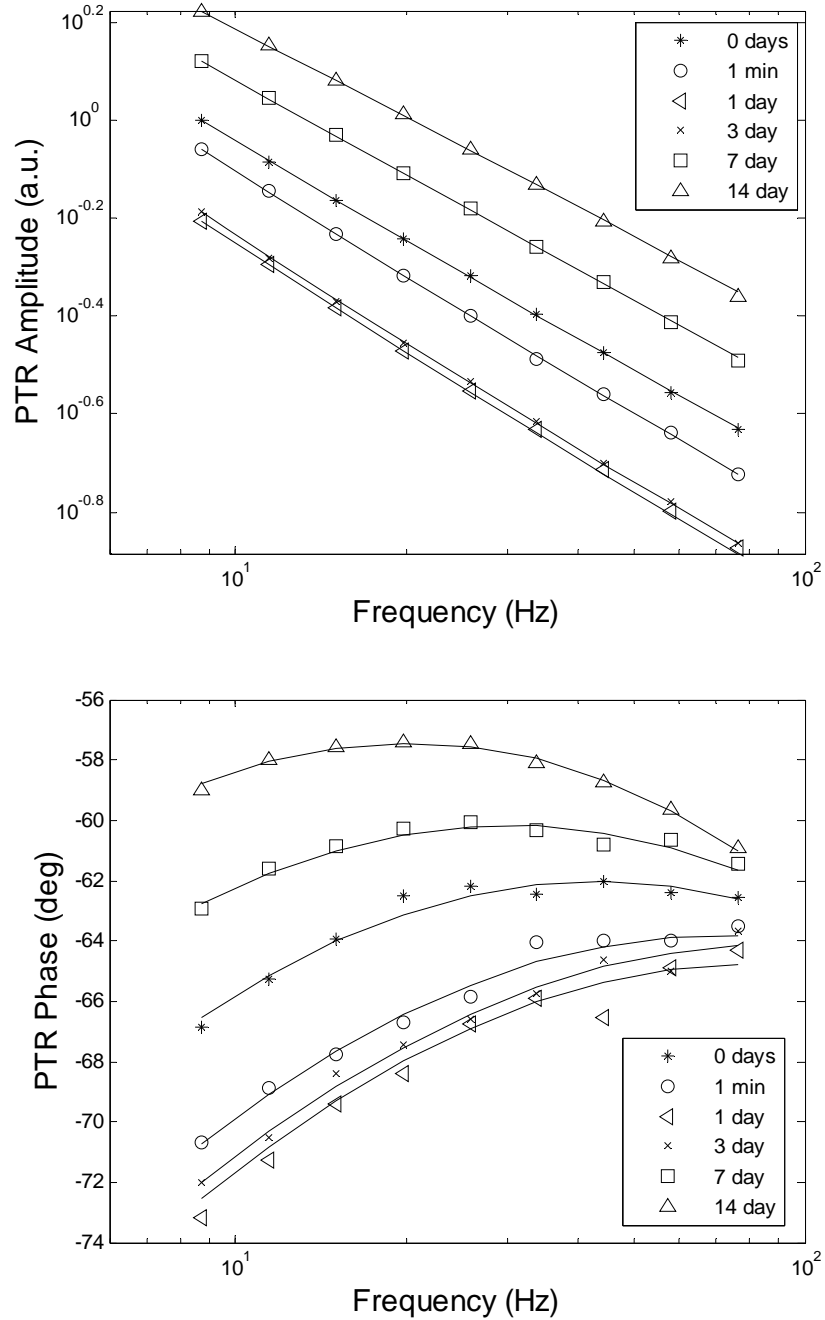


Fig. 3. Amplitude and phase frequency scans for sequential treatment times with corresponding theoretical fits (solid lines).

In the data fitted for 14 days of treatment, the demineralized layer (with the thickness 17 μm measured with TMR) was considered as well. The range of the initially estimated properties of the layer was significantly increased since demineralization can dramatically change the structure of enamel.²¹ The minimal and maximal estimates for the property limits for the remainder of the curves was chosen between the results of the 1 day fits and the results of the 14 days fits. The final results of the fits are shown in Figure 3.

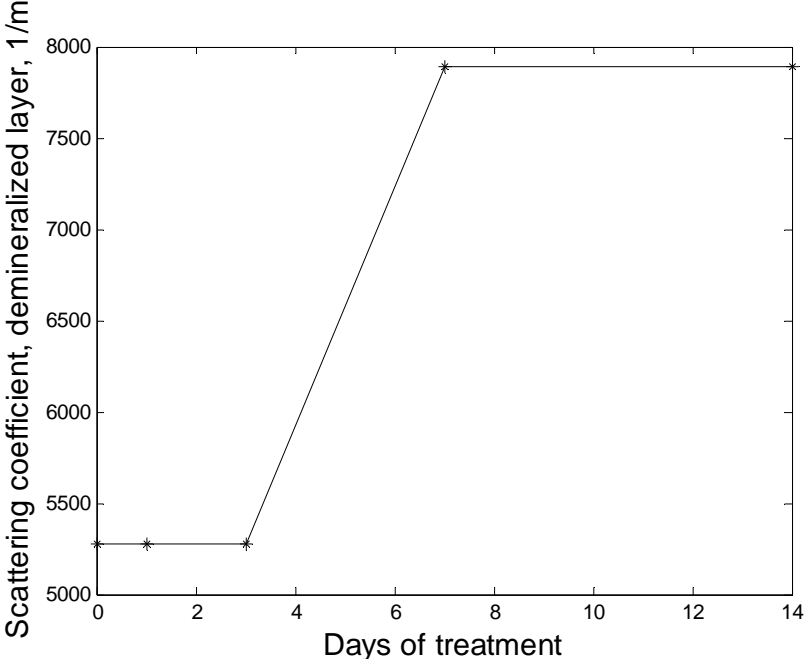


Fig. 4. Optical scattering coefficient of enamel vs. treatment time.

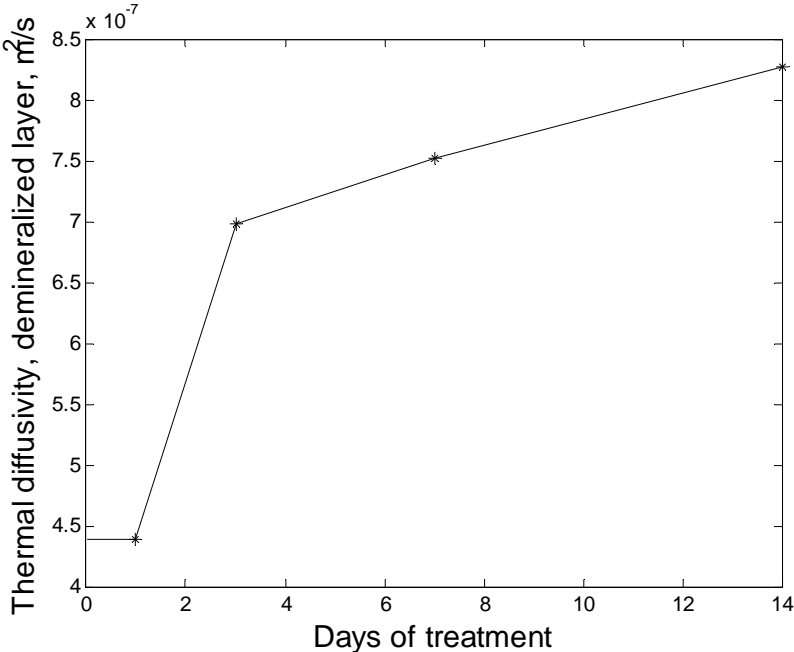


Fig. 5. Thermal diffusivity of enamel vs. treatment time.

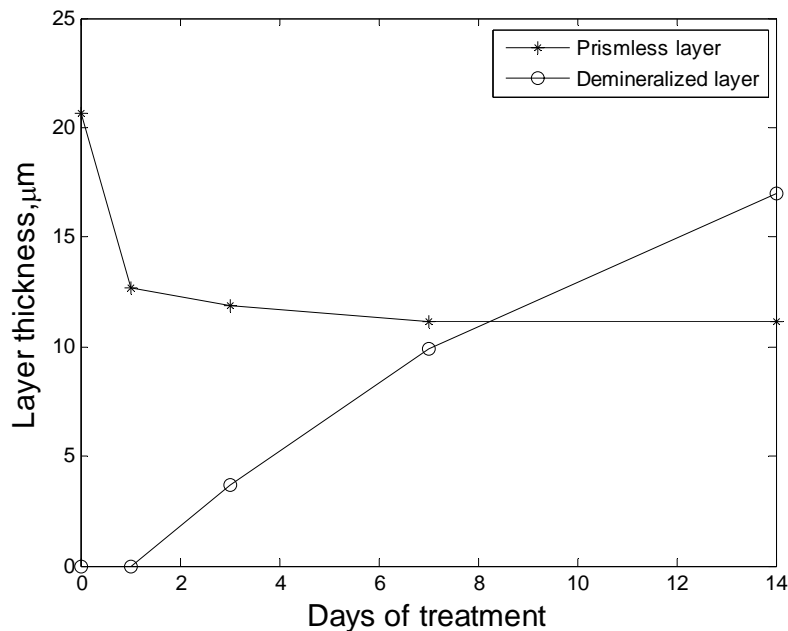


Fig. 6. Thickness of the prismless layer and the demineralized vs. treatment time.

The obtained optical and thermal properties of the layers exhibit behavior consistent with the physical concept of demineralization kinetics. Optical scattering coefficient significantly increased with demineralization (Fig. 4). This trend is well known in the literature²¹ and can be explained by the increase in the micro-porosity of the enamel during demineralization. The thermal diffusivity of the demineralized layer (Fig. 5) also showed a significant increase due to the fact that increasing porosity may involve penetration of air into the structure, which has higher thermal diffusivity. The thickness of the prismless layer (Fig. 6) decreases during treatment since the surface loses mineral, particularly during the first days of treatment. The thickness of the demineralized layer increases monotonically with treatment time (Fig. 6).

In conclusion, the presented methodology can not only evaluate the properties of a multi-layered tissue structure, but can also provide a powerful non-invasive tool for estimating the depth of enamel demineralization. This can be used for the in vivo detection and monitoring of early enamel caries, thus, enhancing the opportunity to prevent and/or impede further mineral loss and accelerate the enamel repair process, prior to cavitation.

REFERENCES

- [1] Patterson M. S., Chance B., and Wilson B. C., "Time resolved reflectance and transmittance for the non-invasive measurement of tissue optical properties", *Appl. Opt.* 28, 2331-2336 (1989).
- [2] Kienle A., Patterson M. S., Dognitz N., Bays R., Wagnieres G., van den Bergh H., "Noninvasive determination of the optical properties of two-layered turbid media", *Appl. Opt.* 37, 779-791 (1998).
- [3] Bevilacqua F., Piguet D., Marquet P., Gross J. D., Tromberg B. J., and Depeursinge C., "In vivo determination of tissue optical properties: application to human brain", *Appl. Opt.* 38, 4939-4950 (1999).
- [4] Ishimaru A., "Diffusion of light in turbid material", *Appl. Opt.* 28, 2210-2215 (1989).
- [5] Farrell T. J., Patterson M. S., Essenpreis M., "Influence of layered tissue architecture on estimates of tissue optical properties obtained from spatially resolved diffuse reflectometry", *Appl. Opt.* 37, 1958-1972 (1998).
- [6] Martelli F., Del Bianco S., and Zaccanti G., "Procedure for retrieving the optical properties of a two-layered medium from time-resolved reflectance measurements", *Opt. Lett.* 28, 1236-1238 (2003).

- [7] Alexandrakis G., Farrell T. J., and Patterson M. S., "Accuracy of the diffusion approximation in determining the optical properties of a two-layer turbid medium", *Appl. Opt.* 37, 7401-7409 (1998).
- [8] Prahl S. A., Vitkin I. A., Bruggemann U., Wilson B. C., and Anderson R.R., "Determination of optical properties of turbid media using pulsed photothermal radiometry", *Phys. Med. Biol.* 37, 1203-1217 (1992).
- [9] Oraevsky A. A., Jacques S. L., Tittel F. K., "Measurements of tissue optical properties by time-resolved detection of laser-induced transient stress", *Appl. Opt.* 36, 402-415 (1997).
- [10] Telenkov S. A., Youn J.-I., Goodman D. M., Welch A. J., and Milner T. E., "Non-contact measurement of thermal diffusivity in tissue", *Phys. Med. Biol.* 46, 551-558 (2001).
- [11] Pichardo-Molina J. L., Gutierrez-Juarez G., Huerta-Franco R., Vargas-Luna M., Cholico P., and Alvarado-Gil J. J., "Open photoacoustic cell technique as a tool for thermal and thermo-mechanical characterization of teeth and their restorative materials", *Int. J. Thermophys.* 26, 243-253 (2005).
- [12] Matvienko A., Mandelis A., Jeon R. J., Abrams S. H., "Theoretical analysis of coupled diffuse-photon-density and thermal-wave field depth profiles photothermally generated in layered turbid dental structures", *J. Appl. Phys.*, in press (2008)
- [13] Nicoalides L., Feng C., Mandelis A., Abrams S. H., "Quantitative dental measurements by use of simultaneous frequency-domain laser infrared photothermal radiometry and luminescence", *Appl. Opt.* 41, 768-777 (2002).
- [14] Fava M., Watanabe I. S., Fava-de-Moraes F., da Costa L. R. R. S., "Prismless enamel in human non-erupted deciduous molar teeth: a scanning electron microscopy study", *Rev. Odontol. Univ. Sao Paulo*, 11(4), 239-24 (1997).
- [15] Kakaboura L. A., Papagiannoulis L., "Bonding of Resinous Materials on Primary Enamel", [Dental Hard Tissues and Bonding: Interfacial Phenomena and Related Properties], Eds. T.Eliades, D. C. Watts, Springer, 35-51 (2005).
- [16] Groenhuis R. A., Ferwerda H. A., and Bosch J. J. T., "Scattering and absorption of turbid materials determined from reflection measurements. 1: Theory", *Appl. Opt.* 22, 2456-2462 (1983).
- [17] Anderson R. R., Beck H., Bruggemann U., Farinelli W., Jacques S. L., and Parrish J., "Pulsed photothermal radiometry in turbid media: internal reflection of backscattered radiation strongly influences optical dosimetry", *Appl. Opt.* 28, 2256-2262 (1989).
- [18] Mandelis A., [Diffusion Wave Fields: Mathematical Methods and Green Functions], Springer New York (2001).
- [19] Amaechi B. T., Higham S. M., and Edgar W. M., "Factors affecting the development of carious lesions in bovine teeth in vitro," *Archs. of Oral Biol.* 43, 619-628 (1998).
- [20] de Josselin de Jong E., ten Bosch J. J., Noordman J., "Optimised microcomputer guided quantitative microradiography on dental mineralized tissue slices," *Phys. Med. Biol.* 32, 887-899 (1987).
- [21] Fried D., Glena R.E., Featherstone J.D.B., and Seka W., "Light scattering properties of natural and artificially demineralized dental enamel at 1310 nm", *Appl. Opt.* 34, 1278-1285 (1995).
- [22] Braden M., "Heat conduction in normal human teeth", *Arch. Oral Biol.* 9, 479-486 (1964).
- [23] Brown W. S., Dewey W. A., and Jacob H. R., "Thermal properties of teeth", *J. Dent. Res.* 49, 752-755 (1970).
- [24] Press W. H., Teukolsky S. A., Vetterling W. T., and Flannery B. P., [Numerical Recipes in Fortran], Cambridge University Press New York (1992).